PROCEEDINGS OF SPIE

SPIEDigitalLibrary.org/conference-proceedings-of-spie

Enhanced second-harmonic generation by single metal–insulator multilayered nanocavities with axial symmetry resonating in the near-infrared

Zilli, Attilio, Isoniemi, Tommi, Iarossi, Marzia, Finazzi, Marco, De Angelis, Francesco, et al.

Attilio Zilli, Tommi Isoniemi, Marzia Iarossi, Marco Finazzi, Francesco De Angelis, Michele Celebrano, Nicolò Maccaferri, "Enhanced second-harmonic generation by single metal–insulator multilayered nanocavities with axial symmetry resonating in the near-infrared," Proc. SPIE 11770, Nonlinear Optics and Applications XII, 117700Y (18 April 2021); doi: 10.1117/12.2589836

SPIE.

Event: SPIE Optics + Optoelectronics, 2021, Online Only

Enhanced second-harmonic generation by single metal–insulator multilayered nanocavities with axial symmetry resonating in the near-infrared

Attilio Zilli[1]*, Tommi Isoniemi[2], Marzia Iarossi[3,4], Marco Finazzi[1], Francesco De Angelis[3], Michele Celebrano[1], and Nicolò Maccaferri[5]*

[1]Department of Physics, Politecnico di Milano, I-20133, Milano, Italy

[2]Department of Physics and Astronomy, University of Sheffield, Sheffield S3 7RH, UK

[3]Istituto Italiano di Tecnologia, I-16163, Genova, Italy

[4]Dipartimento di Informatica, Bioingegneria, Robotica e Ingegneria dei Sistemi (DIBRIS), Università degli Studi di Genova, I-16126 Genova, Italy

[5]Department of Physics and Materials Science, University of Luxembourg, L-1511, Luxembourg, Luxembourg

*attilio.zilli@polimi.it; nicolo.maccaferri@uni.lu

ABSTRACT

We report efficient second-harmonic emission by single multilayer metal–dielectric nanocavities. Engineering the intrinsic interface-induced symmetry breaking by resonant optical absorption design, allows to achieve almost two orders of magnitude higher second-harmonic generation efficiency compared to gold nanostructures with the same geometry. We estimate a second-order nonlinear susceptibility of the order of 1 pm/V, which is comparable to widely used nonlinear crystals. We envision that our system, which combines the advantages of both plasmonic and dielectric materials, might enable the realization of composite nano-systems for an efficient multi-purpose manipulation of nonlinear optical processes at the nanoscale.

Keywords: Metal–dielectric, Multilayers, Nonlinear optics, Second-harmonic generation, Plasmonics, Nanophotonics, Nanocavities, Metamaterials

INTRODUCTION

Multilayered metal–insulator composites are widely used for light confinement[1-3] and guiding at the nanoscale[4,5], as well as manipulation of light scattering and absorption[6,7], optical vortex beam generation at the nanoscale[8], ultrafast all-optical switching[9-11], tailoring optical nonlinearities[12-14], and highly-sensitive detection[15-19]. In this framework, previous theoretical works addressing the second-harmonic generation (SHG)[20-24] mechanism in multilayered metal–insulator systems, identified as the main source of SHG the local symmetry breaking induced at the metal–insulator interfaces. Recently, we reported an experimental study of the full nonlinear optical response, including second- and third-harmonic generation (THG), as well as multi-photon photoluminescence (MPP), of single metal–insulator nanostructures with broken axialsymmetry resonating in the near-infrared spectral region[25]. In this work, we focus instead on the SHG emission

Nonlinear Optics and Applications XII, edited by Mario Bertolotti, Anatoly V. Zayats, Alexei M. Zheltikov, Proc. of SPIE Vol. 11770, 117700Y · © 2021 SPIE
CCC code: 0277-786X/21/$21 · doi: 10.1117/12.2589836

of metal–insulator nanocavities with axial symmetry. The investigated nanostructures can enhance the nonlinear optical response by both engineering the resonant absorption process as well as exploiting the interface-induced local symmetry breaking typical of metal–insulator multilayers. We show that our system provides more than one order of magnitude enhancement of the SHG response compared to pure Au nanoresonators with the same geometry and displaying plasmonic resonances in the same spectral range.

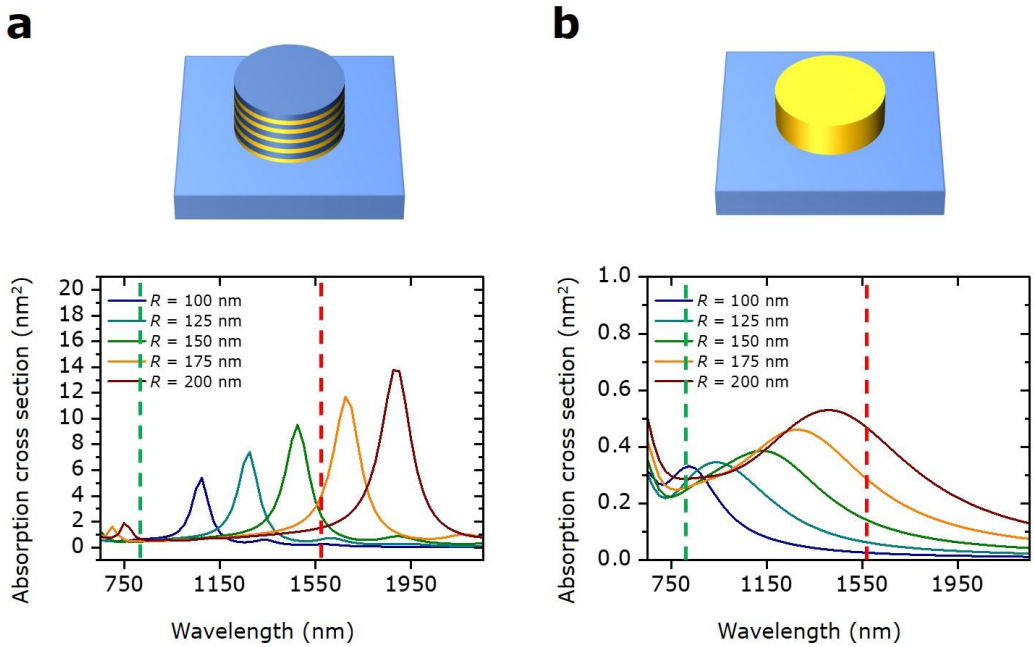

Figure 1 – Calculated optical absorption cross section spectra of (a) metal–insulator nanocavities and (b) Au nanoresonators with varying radii. The dashed red and green lines indicate the fundamental and the second- harmonic wavelength, respectively.

MATERIALS AND METHODS

Multilayered metal–insulator nanocavities made of 5 alternating bi-layers of Au[15 nm]/SiO_2[15 nm] were designed to exhibit strong absorption in the NIR spectral range (Figure 1a) and fabricated by using gallium focused ion beam (FEI Helios NanoLab 650 dual beam system) at 24 pA, milling down to the glass surface around each pillar. The empty milled area around each structure was a circle 3 μm in diameter, and the resulting milling time was 6 min per structure. The nominal radius *R* of the structures spans from 100 nm to 250 nm in steps of 25 nm. Each structure was realized in several replicas to check the reproducibility of the SHG of the single nanostructures. For comparison, we fabricated also bulk Au nanoresonators with the same amount of gold as the metal–insulator nanocavities and resonating in the same spectral range (Figure 1b). Nanoresonators made of SiO_2 were also considered, but not realized and experimentally investigated since they do not display a resonant behavior in this wavelength range and also SiO_2 is not a 2nd order nonlinear medium. The multilayers were deposited on a glass substrate via electron-beam evaporation (Kurt J. Lesker PVD75). The 1 mm-thick glass slide was cleaned with acetone followed by isopropanol, and oxygen plasma cleaning. The 5 bi-layers were deposited sequentially, starting with Au, and capped at the end with aprotective layer of SiO_2 (50 nm). The control samples (bulk Au nanoresonators) were fabricated by depositing 75 nm of Au, namely the same amount of the multilayers, followed by a top layer of 50 nm of SiO_2. The structures were imaged with scanning electron microscopy in the same system after milling.

To simulate the optical properties of the metal–insulator nanocavities we used the finite- element method as implemented in a commercial solver (Comsol Multiphysics). We solved the electromagnetic wave equation in the frequency domain, that is, looking for stationary solutions. This is justified, inasmuch as the electron dynamics underpinning the nonlinear response is much faster (few fs) than the pulse duration in experiments. We considered a simulation region 2 μm x 2 μm x 4 μm, where the exciting electromagnetic field was a linearly polarized plane wave propagating perpendicularly to the

substrate. The frequency-dependent permittivities of gold and SiO_2 have been taken from literature[26,27]. We then calculated the field scattered by a single nanocavity to extract observables such as the optical absorption.

The nonlinear optical measurements were performed on single nanostructures using a home-built nonlinear microscope coupled with a laser delivering ultrafast pulses (τ_{pulse} = 160 fs, f_{rep} = 80 MHz) centered at the fundamental wavelength (FW) λ = 1554 nm (see Figure 2). The pump beam was focused with a 0.85 NA air objective producing a 2.2 μm diffraction-limited spot size. All the experiments were performed with 500 μW average pump power at the sample (peak intensity 1 GW/cm^2). The SHG signal is then collected and sent to a spectrometer (Andor, Shamrock SR303i) equipped with a CCD camera (Andor iKon-M DU934P-BV) to acquire the emission spectrum. Alternatively, the SHG signal is chromatically filtered and focused onto a silicon single-photon avalanche diode (SPAD) (Micro Photon Devices, PD-050-CTD) for high-sensitivity detection. The sample is mounted on a piezoelectric stage, which allows scanning the structure under the beam to acquire spatial maps of the nonlinear emission.

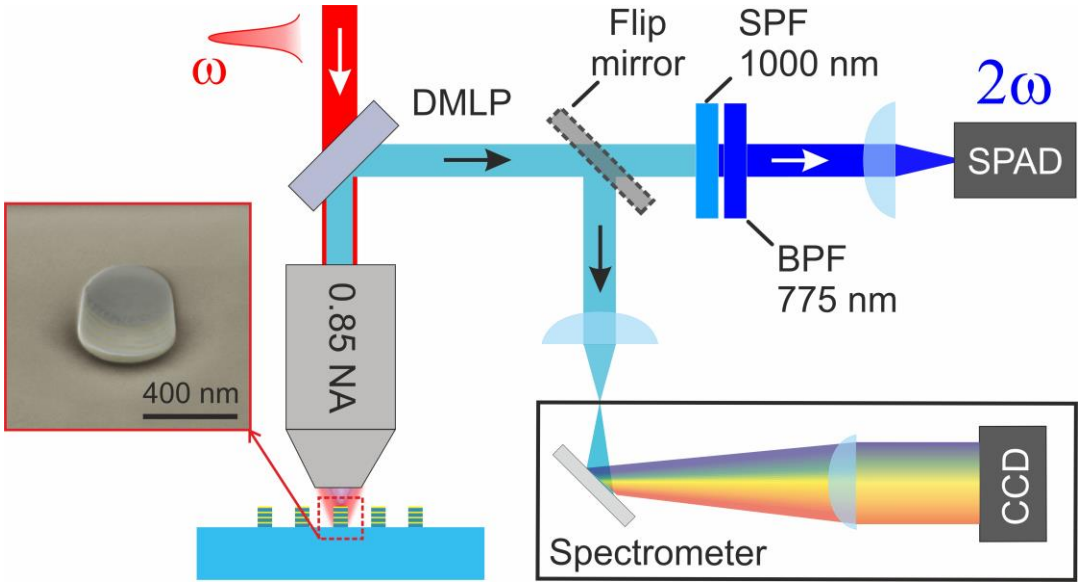

Figure 2 – Sketch of the nonlinear microscope used in the experiments. Acronym key: DMLP = dichroic mirror, long pass; SPF = short- pass filter; BPF = band-pass filter; NA = numerical aperture; CCD = charge-coupled device. The inset on the left is a scanning electron micrograph a multilayer structure, with the gold layers colored by hand with a golden hue.

Let us now introduce some metrics we adopted for quantifying the nonlinear performance of the nanostructures. To estimate the conversion efficiency

$$\eta_{\mathrm{SHG}} \equiv \frac{P_{\mathrm{SHG}}^{\mathrm{out}}}{P_{\mathrm{FW}}^{\mathrm{in}}}$$

where $P_{\mathrm{FW}}^{\mathrm{in}} = 500\ \mu\mathrm{W}$ is the time-averaged pump power used in experiments, we used the following procedure. We first estimated nonlinear coefficient

$$\gamma_{\mathrm{SHG}} = \frac{\hat{P}_{\mathrm{SHG}}^{\mathrm{out}}}{\left(\hat{P}_{\mathrm{FW}}^{\mathrm{in}}\right)^2}$$

obtained by dividing the peak powers of the emitted nonlinear signal $\hat{P}_{\mathrm{SHG}}^{\mathrm{out}}$ by the square $\left(\hat{P}_{\mathrm{FW}}^{\mathrm{in}}\right)^2$ of the impinging powers respectively, where $\hat{P} = P/f_{\mathrm{rep}}\Delta\tau_{\mathrm{pulse}}$. In fact, these coefficients are independent from both the repetition rate, f_{rep}, and pulse width, $\Delta\tau_{\mathrm{pulse}}$, of the excitation pulses. The light emitted by the nanostructure within the solid angle of detection of the objective is 70% of the total, since we collect from the higher refractive index half-space. The light transmitted by the

microscope objective is 85%, while the metallic mirrors and the dichroic mirror reflects 96% and 99% respectively. The quantum efficiency of the SPAD is 15% at 777 nm, while the light effectively collected by the SPAD (filling factor) is 50%, due to the finite size of the device (50 μm). Therefore, the overall optical throughput is 4%, without taking into account further losses due to cropping in the detection path.
We derived also the *effective* nonlinear susceptibility

$$\chi_{\mathrm{eff}}^{(2)} = \sqrt{\hat{\gamma}_{\mathrm{SHG}} \frac{3\pi\epsilon_0 c A_{\mathrm{eff}}^2}{k^4 V^2}}$$

which quantifies the SHG performance of the nanocavity independently from the experimental configuration, but do not correspond to the local $\chi_{\mathrm{eff}}^{(2)}$ of the materials since they do not account for the inhomogeneous distribution of the nonlinear sources both in the volume and at the surface of the nanocavity. Here, $A_{\mathrm{eff}} = \pi \times (0.67 \times 1554\ \mathrm{nm}/0.85)^2 = 4.7 \times 10^{-12}\ \mathrm{m}^2$ is the area of the diffraction-limited pump, $V = \pi \times (200\ \mathrm{nm})^2 \times 400\ \mathrm{nm} = 5.0 \times 10^{-20}\ \mathrm{m}^3$ is the volume of the most resonant structures, and k is the wavevector of the incoming beam in vacuum.

RESULTS AND DISCUSSION

In our experimental conditions, the Au nanoresonators do not yield any detectable SHG signal. Only a radial cut, breaking the axial symmetry, brings about a sizeable SHG in the Au nanoresonators, as previously shown in Ref. [25] and Ref. [28]. On the contrary, metal–insulator nanocavities produce a steady SHG. This can be appreciated in figure 3a, which shows the emission spectrum of a single multilayer structure with radius R = 175 nm. The SHG and THG peak are visible at 777 nm and 518 nm respectively, whereas the broad emission band between them is due to MPP. The dependence of the SHG power on R is shown in Fig. 3b. In particular, we have estimated the SHG signal enhancement by evaluating the count rates in the maps collected on the metal–insulator nanostructures. The SHG signal detected on the most resonant particle is 15 kcts/s. Conversely, the SHG signal from the homogeneous Au nanoresonators was not detectable. A lower-bound estimate on the SHG enhancement from the multilayered compared to the homogenous nanoresonators can be attained by assuming the SHG from the latter to be of order of detector dark counts (0.1 kcts/s). This allows to estimate more than two order of magnitude SHG enhancement due to both multilayering and field confinement in the MMD nanoantenna. Concurrently, we evaluated the enhancement factor induced by the sole multilayering, by comparing the SHG yield from the bulk Au continuous film (0.5 kcts/s) with that of the metal–insulator one (6 kcts). This clearly stress the fact the one order of magnitude enhancement factor can be attributed to the multilayering. Therefore, we conclude that shaping metal–insulator layers into resonant nanostructures allows one to further boost the enhancement by at least one order of magnitude, while considerably reducing the material fingerprint. To summarize, we can therefore ascribe the observed enhancement to the combination of two main mechanisms: (i) the local breaking of the inversion symmetry at the metal–insulator interfaces and (ii) the presence of a strong absorption peak at the FW, which is almost absent in the gold nanoresonators typical of these metal–insulator nanocavities[6] (see Figure 1a and 1b). In other terms, by comparing the SHG yield of the multilayered film with that of the nanoresonantor, we find about a factor 3 enhancement factor. However, by considering a laser spot area of about 4 μm^2 (beam radius ~1.2 μm) and a nanoresonator spatial fingerprint of about 0.1 μm^2, we obtain a 40 times smaller illuminated volume for the nanoresonator, which allows us to conclude that the field confinement obtained brings about a two orders of magnitude enhancement. Considering the SHG emission by the most efficient metal–insulator nanocavity in the experiment (i.e. R = 175 nm) and accounting for the optical losses in the detection path retrieve the total emitted power, we experimentally estimate an effective second-order nonlinear susceptibility $\chi^{(2)}_{\mathrm{eff}}$ = 1.7 pm/V, which is comparable to some widely-employed second-order upconverting nonlinear crystals, such as potassium di-deuterium phosphate (KDP)[29]. Moreover, we found for the best metal–insulator nanocavity a conversion efficiency of $\eta_{\mathrm{SHG}} \cong 5 \times 10^{-10}$, corresponding to a nonlinear coefficient of $\gamma_{\mathrm{SHG}} \cong 8 \times 10^{-12}\ W^{-1}$. On the other hand, we could not detect SHG from the bulk gold nanostructure; consequently, for these structures the detection noise level constitutes an upper bound to the efficiency equal to $\eta_{\mathrm{SHG}} \sim 10^{-11}$, corresponding to $\gamma_{\mathrm{SHG}} \sim 4 \times 10^{-13}\ W^{-1}$. To evaluate the effect of the geometrical confinement (resonance tuning), we performed a systematic study of the SHG response of the individual metal–insulator nanocavities with radius increasing from 100 nm to 250 nm in steps of 25 nm. The measured SHG power, averaged over 10 nominally identical replicas of each structure, is reported in Figure 3b. The error bars, representing the standard error of the mean, reflect the role of random defects introduced by the nanofabrication process, such as roughness in the thin films due to e-beam deposition and radiation damage induced by the gallium beam.

In our metal–insulator nanocavities, the SHG response is maximum for a radius of 175 nm, indicating that the emission is dominated by the resonant behavior at the FW (Figure 1a and Figure 3c). In fact, by inspecting the radius dependence of σ_{abs} at the FW, we see that its maximum matches quite closely the SHG power maximum, and a resonant dependent SHG can be explained with this simple argument, that is the geometrical confinement of the metal–insulator system. The slight shift towards lower radii (red-shift in wavelength) of the experimental result compared to the calculated peak could be due to several reasons, for instance the slight variation between the shape of the simulated structures and the non-ideal conical shape of the experimental structures, as well as the use of a plane wave in the simulations, which does not reproduce exactly the experimental illumination (focused beam) in the experiments. Finally, a simple approach to model the SH emission from these structures, based on the Miller's rule[30,31], is to combine the calculated radius-dependent linear cross sections into the nonlinear coefficient $\epsilon^{(2)} \equiv \sigma_{abs}(\omega)^2 \sigma_{sca}(2\omega)$, assuming that the nonlinear process is governed by absorption at the FW, and by scattering at the SHG wavelength. These coefficients account only for the coupling strength between the antenna and the radiation at the excitation and emission wavelengths. This description of the process does not consider the spatial overlap between the fields[32] at the two wavelengths of interest and the relative polarization enabled by the selection rules for the nonlinear processes. The measured nonlinear emission trend (Figure 3b) is in qualitative good agreement with the computed nonlinear coefficients (Figure 3d), thereby highlighting the key role played by the absorption resonance at the FW.

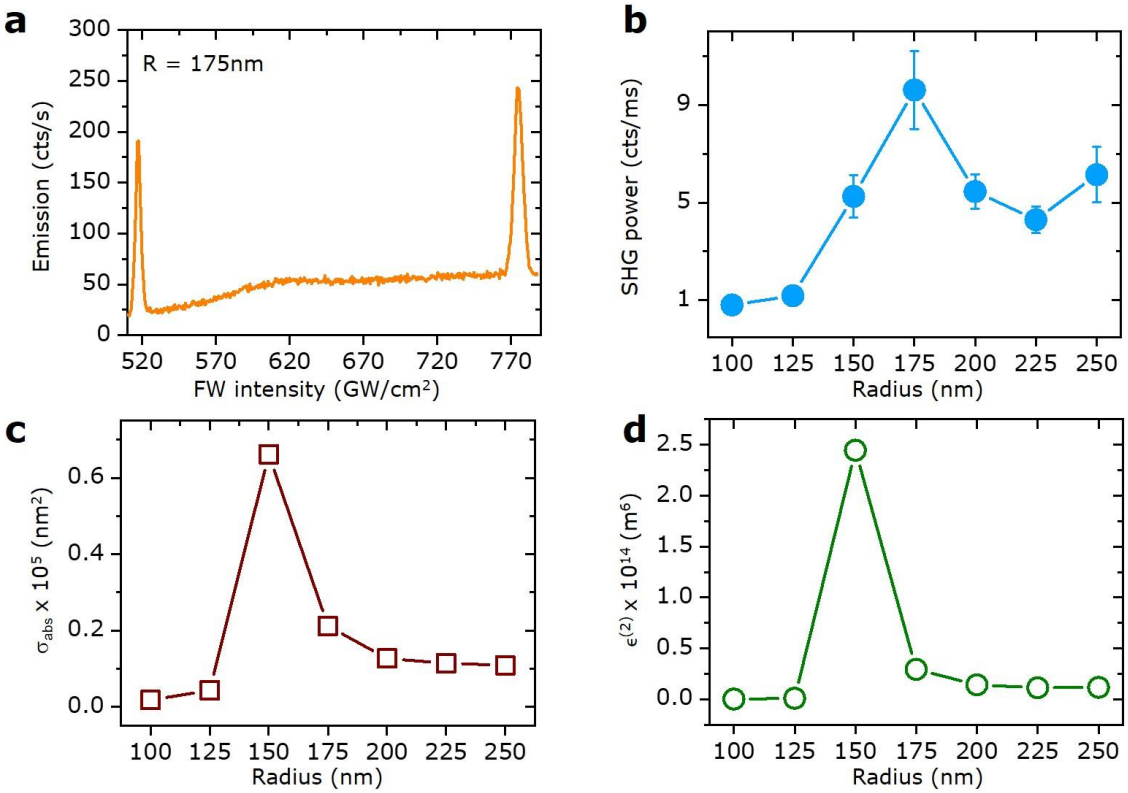

Figure 3 – (a) Nonlinear emission spectrum of a single multilayer structure of radius R = 175 nm. (b) SHG power (most intense pixel of the confocal image of the structure) of the MMD nanocavities. Each plotted point is the mean measured over 10 nominally identical replicas, and the error bars correspond to the standard error of the mean. The signals are collected using an illumination average power of about 500 μW (pulse peak intensity 1 GW/cm^2). (c) Calculated absorption cross-section at the FW as a function of R. (d) Calculated nonlinear coefficient $\epsilon^{(2)}$ as a function of R.

CONCLUSIONS

We reported efficient second-harmonic emission by multilayered metal–insulator nanocavities, where the absorption at the fundamental wavelength is enhanced by tailoring the geometry of the structures, and boosts the nonlinear optical generation beyond the contribution of the interface-induced symmetry breaking. Moreover, the axial symmetry of the

system makes that the generated second harmonic largely independent from the exciting polarization. Notably, we found that in our experimental conditions the second-harmonic emission is more than one order of magnitude larger than that of pure Au nanostructures with the same geometry and resonant behavior. We emphasize that these structures can be fabricated on a large scale by using hole-mask colloidal lithography also to achieve complicated structures[7], and detached from the substrate[33]. Albeit beyond the scope of this work, we foresee that these structures can be used as nonlinear probes in biological systems, where it is fundamental to control the emission of visible light from probes that resonate in the NIR spectral range in correspondence to the biological transparency window, which allows to image probes located deep in the tissue. In this context, the choice of materials is important to provide high values of $\chi^{(2)}$ or $\chi^{(3)}$. We have found that our nonlinear susceptibilities are of the same order of magnitude of common nonlinear optical crystals, such as potassium dihydrogenphosphate (KH_2PO_4). Other materials, such as lithium niobate ($LiNbO_3$), barium titanate ($BaTiO_3$), bismuth ferrite ($BiFeO_3$), though having higher $\chi^{(2)}$ values, are not well-suited for *in-vivo* imaging due to their cytotoxicity[34,35]. On the contrary, Au nanoparticles and dielectric materials such as SiO_2 are widely used in nanomedicine thanks to their biocompatibility[36]. Finally, an exciting perspective for these multilayered architectures would be combining their nonlinear optical properties with those of quantum emitters[1] or 2D materials such as transition metal dichalcogenides[37].

REFERENCES

[1] Indukuri, S. R. K. C., Bar-David, J., Mazurski, N. and Levy, U., "Ultrasmall mode volume hyperbolic nanocavities for enhanced light–matter interaction at the nanoscale," ACS Nano 13(10), 11770–11780 (2019).

[2] Zhumabek, T. and Valagiannopoulos C., "Light trapping by arbitrarily thin cavities," Phys. Rev. Research 2, 043349 (2020).

[3] Garoli, D., Calandrini, E., Bozzola, A., Toma, A., Cattarin, S., Ortolani, M. and De Angelis, F., "Fractal-Like Plasmonic Metamaterial with a Tailorable Plasma Frequency in the near-Infrared," ACS Photonics 5, 3408–3414 (2018).

[4] Dionne, J. A., Sweatlock, L. A., Atwater, H. A. and Polman, A., "Planar metal plasmon waveguides: frequency-dependent dispersion, propagation, localization, and loss beyond the free electron model," Phys. Rev. B 72, 075405 (2005).

[5] Maccaferri, N., Isoniemi, T., Hinczewski, M., Iarossi, M., Strangi, G. and De Angelis, F., "Designer Bloch plasmon polariton dispersion in grating-coupled hyperbolic metamaterials," APL Photonics 5(7), 076109 (2020).

[6] Isoniemi, T., Maccaferri, N., Ramasse, Q. M., Strangi, G. and De Angelis, F., "Electron energy loss spectroscopy of bright and dark modes in hyperbolic metamaterial nanostructures," Adv. Opt. Mater. 8(13), 2000277 (2020).

[7] Maccaferri, N., Zhao, Y., Isoniemi, T., Iarossi, M., Parracino, A., Strangi, G. and De Angelis, F., "Hyperbolic meta-antennas enable full control of scattering and absorption of light," Nano Lett. 19(3), 1851−1859 (2019).

[8] Garoli, D., Zilio, P. Gorodetski, Y., Tantussi, F. and De Angelis, F., "Optical vortex beam generator at nanoscale level," Sci. Rep. 6, 29547 (2016).

[9] Kuttruff J., Garoli, D., Allerbeck, J., Krahne, R., De Luca, A., Brida, D., Caligiuri, V. and Maccaferri, N., "Ultrafast all-optical switching enabled by epsilon-near-zero modes in metal-insulator nanocavities," Commun. Phys. 3, 114 (2020).

[10] Caligiuri, V., Pianelli, A., Miscuglio, M., Patra, A., Maccaferri, N., Caputo, R. and De Luca, A., "Near- and mid-infrared graphene-based photonic architectures for ultrafast and low-power electro-optical switching and ultra-high resolution imaging," ACS Appl. Nano Mater. 3(12), 12218–12230 (2020).

[11] Rashed, A. R., Yildiz, B. C., Ayyagari, S. R. and Caglayan, H., "Hot electron dynamics in ultrafast multilayer epsilon-near-zero metamaterials," Phys. Rev. B 101, 165301 (2020).

[12] Suresh, S., Reshef, O., Alam, M. Z., Upham, J., Karimi, M. and Boyd, R. W., "Enhanced nonlinear optical responses of layered epsilon-near-zero metamaterials at visible frequencies," ACS Photonics 8(1), 125-129 (2021).

[13] Wenyang, W., Fan, L., Zang, W., Yang, X., Zhan, P., Chen, Z. and Wang, Z., "Second harmonic generation enhancement from a nonlinear nanocrystal integrated hyperbolic metamaterial cavity," Opt. Express 25(18), 21342-21348 (2017).

[14] Ortolani, M., Mancini, A., Budweg, A., Garoli, D., Brida, D. and De Angelis, F., "Pump-probe spectroscopy study of ultrafast temperature dynamics in nanoporous gold," Phys. Rev. B 99, 035435 (2019).

[15] Sreekanth, K. V., Alapan, Y, ElKabbash, M., Ilker, E., Hinczewski, M., Gurkan, U. A., De Luca, A. and Strangi, G., "Extreme sensitivity biosensing platform based on hyperbolic metamaterials," Nat. Mater. 15, 621–627 (2016).

[16] Palermo, G., Sreekanth, K. V., Maccaferri, N., Lio, G. E., Nicoletta, G., De Angelis, F., Hinczewski, M. and Strangi, G. "Hyperbolic dispersion metasurfaces for molecular biosensing," Nanophotonics 10(1), 295–314 (2021).

[17] Garoli, D., Calandrini, E., Giovannini, G., Hubarevich, A., Caligiuri, V. and De Angelis, F., "Nanoporous gold metamaterials for high sensitivity plasmonic sensing," Nanoscale Horiz. 4, 1153–1157 (2019).

[18] Maccaferri, N., Barbillon, G., Koya, A. N., Lu, G., Acuna, G. P. and Garoli, D., "Recent advances in plasmonic nanocavities for single-molecule spectroscopy," Nanoscale Adv. 3, 625–632 (2021).

[19] Carrara, A., Maccaferri, N., Cerea, A., Bozzola, A., De Angelis, F., Proietti Zaccaria, R. and Toma, A., "Plasmon hybridization in compressible metal–insulator–metal nanocavities: an optical approach for sensing deep sub-wavelength deformation," Adv. Opt. Mater. 8(18), 2000609 (2020).

[20] Duncan, C., Perret, L., Palomba, S., Lapine, M., Kuhlmey, B. T. and Martijn de Sterke, C., "New avenues for phase matching in nonlinear hyperbolic metamaterials," Sci. Rep., 5, 8983 (2015).
[21] Sun, Y., Zheng, Z., Cheng, J., Sun, G. and Qiao, G., "Highly efficient second harmonic generation in hyperbolic metamaterial slot waveguides with large phase matching tolerance," Opt. Express, 23(5), 6370–6378 (2015).
[22] Vincenti, M. A., Kamandi, M., de Ceglia, D., Guclu, C., Scalora, M. and Capolino, F., "Second-harmonic generation in longitudinal epsilon-near-zero materials," Phys. Rev. B 96, 045438 (2017).
[23] Pakhomov, A. V., Hammerschmidt, M., Burger, S., Pertsch, T. and Setzpfandt, F., " Modeling of surface-induced second-harmonic generation from multilayer structures by the transfer matrix method," Opt. Express 29(6), 9098–9122 (2021).
[24] Wu, W., Fan, L., Zang, W., Yang, X., Zhan, P., Chen, Z. and Wang, Z., "Second harmonic generation enhancement from a nonlinear nanocrystal integrated hyperbolic metamaterial cavity," Opt. Express 25(18), 21342–21348 (2017).
[25] Maccaferri, N., Zilli, A., Isoniemi, T., Ghirardini, L., Iarossi, M., Finazzi, M., Celebrano, M. and De Angelis, F., "Enhanced nonlinear emission from single multilayered metal–dielectric nanocavities resonating in the near-infrared," ACS Photonics 8(2), 512–520 (2021).
[26] Rakić, A. D.; Djurišic, A. B.; Elazar, J. M.; Majewski, M. L. Optical properties of metallic films for vertical-cavity optoelectronic devices. *Appl. Opt.* **1998**, *37*, 5271-5283.
[27] Malitson. I. H. Interspecimen Comparison of the Refractive Index of Fused Silica. *J. Opt. Soc. Am.* **1965**, *55*, 1205-1208.
[28] Sartorello, G., Olivier, N., Zhang, J., Yue, W., Gosztola, D. J., Wiederrecht, G. P., Wurtz, G. and Zayats, A. V., "Ultrafast optical modulation of second- and third-harmonic generation from cut-disc-based metasurfaces," ACS Photonics, 3(8), 1517–1522 (2016).
[29] Dmitriev, V. G., Gurzadyan, G. G. and Nikogosyan, D. N. “Handbook of nonlinear optical crystals”, Springer, Third Edition (1999).
[30] Garrett, C. and Robinson, F., "Miller’s phenomenological rule for computing nonlinear susceptibilities," IEEE J. Quantum Electron. 2(8), 328–329 (1966).
[31] Miller, R. C., "Optical second harmonic generation in piezoelectric crystals," Appl. Phys. Lett. 5, 17–19 (1964).
[32] Celebrano, M., Wu, X., Baselli, M., Großmann, S., Biagioni, P., Locatelli, A., De Angelis, C., Cerullo, G., Osellame, R., Hecht, B., Duò, L., Ciccacci, F. and Finazzi, M., “Mode matching in multiresonant plasmonic nanoantennas for enhanced second harmonic generation,” Nat. Nanotechnol. 10, 412−417 (2015).
[33] Lodewijks, K., Miljkovic, V., Massiot, I., Mekonnen, A., Verre, R., Olsson, E. and Dmitriev, A., " Multiscale conformal pattern transfer," Sci. Rep. 6, 28490 (2016).
[34] Staedler, D., Magouroux, T., Hadji, R. Joulaud, C., Extermann, J., Schwung, S., Passemard, S., Kasparian, C., Clarke, G., Gerrmann, M., Le Dantec, R., Mugnier, Y., Rytz, D., Ciepielewski, D., Galez, C., Gerber-Lemaire, S., Juillerat-Jeanneret, L., Bonacina, L. and Wolf, J.-P., "Harmonic nanocrystals for biolabeling: a survey of optical properties and biocompatibility," ACS Nano 6(3), 2542–2549 (2012).
[35] Grange, R., Lanvin, T., Hsieh, C.-L., Pu, Y. and Psaltis, D., "Imaging with second-harmonic radiation probes in living tissue," Biomed. Opt. Express 2(9), 2532–2539 (2011).
[36] Dreaden, E. C., Alkilany, A. M., Huang, X., Murphy, C. J. and El-Sayed, M. A., “The golden age: gold nanoparticles for biomedicine,” Chem. Soc. Rev. 41, 2740−2779 (2012).
[37] Chaitanya Indukuri, S. R. K., Frydendahl, C., Bar-David, J., Mazurski, N. and Levy, U., "WS2 monolayers coupled to hyperbolic metamaterial nanoantennas: broad implications for light–matter-interaction applications," ACS Appl. Nano Mater. 3(10), 10226–10233 (2020).